Physics Letters B 804 (2020) 135352

Contents lists available at ScienceDirect

Physics Letters B

www.elsevier.com/locate/physletb

QCD at finite isospin density: Chiral perturbation theory confronts lattice data

Prabal Adhikari [a,b], Jens O. Andersen [b,c,*]

[a] Wellesley College, Department of Physics, 106 Central Street, Wellesley, MA 02481, United States
[b] Department of Physics, Norwegian University of Science and Technology, Høgskoleringen 5, N-7491 Trondheim, Norway
[c] Niels Bohr International Academy, Blegdamsvej 17, DK-2100 Copenhan, Denmark

ARTICLE INFO

Article history:
Received 19 September 2019
Received in revised form 6 February 2020
Accepted 2 March 2020
Available online 10 March 2020
Editor: J.-P. Blaizot

Keywords:
Chiral perturbation theory
Finite isospin
QCD

ABSTRACT

We consider the thermodynamics of three-flavor QCD in the pion-condensed phase at nonzero isospin chemical potential (μ_I) and vanishing temperature using chiral perturbation theory in the isospin limit. The transition from the vacuum phase to a superfluid phase with a Bose-Einstein condensate of charged pions is shown to be second order and takes place at $\mu_I = m_\pi$. We calculate the pressure, isospin density, and energy density to next-to-leading order in the low-energy expansion. Our results are compared with recent high-precision lattice simulations as well as previously obtained results in two-flavor chiral perturbation theory. The agreement between the lattice results and the predictions from three-flavor chiral perturbation theory is very good for $\mu_I < 200$ MeV. For larger values of μ_I, the agreement between lattice data and the two-flavor predictions is surprisingly good and better than with the three-flavor predictions. Finally, in the limit $m_s \gg m_u = m_d$, we show that the three-flavor observables reduce to the two-flavor observables with renormalized parameters. The disagreement between the results for two-flavor and three-flavor χPT can largely be explained by the differences in the measured low-energy constants.

1. Introduction

QCD in extreme conditions, i.e. high temperature and density has received a lot of attention in the past decades due to its relevance to the early universe, heavy-ion collisions, and compact stars [1–3]. For example, QCD at finite baryon density (μ_B) is of significant interest since the equation of state (EoS) is used as input for calculating the macroscopic properties of neutron stars. However, lattice QCD cannot be applied to QCD at nonzero baryon density due to the sign problem: integrating out the fermions in the path integral for the partition function gives rise to a functional determinant that can be considered part of the probability measure. At $\mu_B \neq 0$, this determinant is complex and standard Monte Carlo techniques cannot be applied. A way to circumvent this problem, for high temperatures and small chemical potentials, is by Taylor expanding the thermodynamic quantities about zero μ_B [4]. For small T and large μ_B, this is obviously hopeless. Due to asymptotic freedom, we expect to be able to use weak-coupling techniques at very high densities [5,6]. In the weak-coupling expansion the series is now known to order α_s^2 for massive quarks [7] and $\alpha_s^3 \log^2 \alpha_s$ for massless quarks [8]. For lower densities, where weak-coupling techniques do not apply, we have to use low-energy models of QCD, see Ref. [9] for a recent review.

There are variants of QCD that do not suffer from the sign problem. These include two-color QCD [10], three-color QCD with fermions in the adjoint representation [11], zero density QCD in an external magnetic field [12], and three-color QCD at finite isospin [13–17]. The absence of the sign problem implies that one can simulate these systems on the lattice and compare the results with low-energy models and theories. In the case of QCD at finite isospin chemical potential, one finds at $T = 0$, a transition from the vacuum to a pion-condensed phase at a critical isospin chemical potential $\mu_I^c = m_\pi$. The mechanism of pion condensation and the transition to a pion superfluid phase out of the vacuum is simply that it is energetically favorable to form such a condensate for $\mu_I \geq \mu_I^c$. Moreover, with increasing isospin chemical potential, it is expected that there is a crossover to a BCS phase. Since the order parameter in the BCS phase has the same quantum numbers as a charged pion condensate, this is not a true phase transition, but associated with the formation of a Fermi surface and subsequent condensation of Cooper pairs. A very recent review on meson condensation can be found in Ref. [18].

* Corresponding author at: Department of Physics, Norwegian University of Science and Technology, Høgskoleringen 5, N-7491 Trondheim, Norway.
E-mail address: andersen@tf.phys.ntnu.no (J.O. Andersen).

https://doi.org/10.1016/j.physletb.2020.135352

Chiral perturbation theory (χPT) is a low-energy effective theory of QCD based only on its global symmetries and the degrees of freedom, and the predictions of χPT are, therefore, model independent [19–22]. It has been remarkably successful in describing the phenomenology of the pseudo-Goldstone bosons that result from the spontaneous breakdown of chiral symmetry in the QCD vacuum. χPT at finite isospin was first considered by Son and Stephanov in their seminal paper two decades ago [23], in which all the leading order results were derived.

In this letter, we calculate the effective potential in chiral perturbation theory at next-to-leading (NLO) order in the low-energy expansion for three flavors at finite isospin chemical potential. While the phase diagram as functions of isospin and strange chemical potentials (μ_S) has been mapped out and leading order (LO) thermodynamic functions have been known for two decades [23,24], the leading quantum corrections at finite μ_I are presented here for the first time, however, see Ref. [25] for some partial NLO results in two-color QCD and Refs. [26–32] for various aspects of χPT for three-color QCD including some NLO effects. Finite isospin systems have also been studied in the context of low-energy effective models including the non-renormalizable Nambu-Jona-Lasinio model [33–47], and the renormalizable quark-meson model [48–51].

We derive the pressure, isospin density, and equation of state, and compare these quantities with recent lattice results as well earlier results from two-flavor χPT [52]. In the large-m_s limit, the three-flavor result is matched onto the two-flavor result of Ref. [52] with renormalized parameters. The disagreement between the two-flavor and three-flavor results are discussed and shown to be related to the differences in the experimental values of the low-energy constants. Results on the thermodynamics of the kaon-condensed phases at finite μ_S and μ_I as well as calculational details can be found in an accompanying long paper [53].

2. Chiral perturbation theory

As mentioned above, χPT is an effective low-energy theory of QCD based solely on its global symmetries and low-energy degrees of freedom. In massless three-flavor QCD, the symmetry is $SU(3)_L \times SU(3)_R \times U(1)_B$, which in the vacuum is broken down to $SU(3)_V \times U(1)_B$. For two degenerate light quarks, the symmetry is $SU(2)_I \times U(1)_Y \times U(1)_B$. If we add a quark chemical potential for each flavor, the symmetry is $U(1)_{I_3} \times U(1)_Y \times U(1)_B$. In three-flavor QCD, we keep the octet of mesons, which implies that chiral perturbation theory is not valid for arbitrarily large chemical potential. Considering the hadron spectrum, one naively expects that the expansion is valid for $|\mu_u| = |\mu_d| < 300$ MeV [24]. χPT has a well defined power counting scheme, where each derivative as well as each factor of a quark mass counts as one power of momentum p. At leading order in momentum, $\mathcal{O}(p^2)$, there are only two terms in the chiral Lagrangian

$$\mathcal{L}_2 = \frac{f^2}{4}\mathrm{Tr}\left[\nabla_\mu \Sigma^\dagger \nabla^\mu \Sigma\right] + \frac{f^2}{4}\mathrm{Tr}\left[\chi^\dagger \Sigma + \chi \Sigma^\dagger\right], \tag{1}$$

where f is the bare pion decay constant, $\chi = 2B_0 M$,

$$M = \mathrm{diag}(m_u, m_d, m_s) \tag{2}$$

is the quark mass matrix and $\Sigma = U\Sigma_0 U$, where $U = \exp\frac{i\lambda_i\phi_i}{2f}$ and $\Sigma_0 = \mathbb{1}$ is the vacuum. Here λ_i are the Gell-mann matrices that satisfy $\mathrm{Tr}\lambda_i\lambda_j = 2\delta_{ij}$ and ϕ_i are the fields parametrizing the Goldstone manifold ($i = 1, 2..., 8$). In the remainder we work in the isospin limit, $m = m_u = m_d$. The covariant derivative and its Hermitian conjugate at nonzero quark chemical potentials, μ_q ($q = u, d, s$), are defined as follows

$$\nabla_\mu \Sigma \equiv \partial_\mu \Sigma - i[v_\mu, \Sigma], \tag{3}$$

$$\nabla_\mu \Sigma^\dagger = \partial_\mu \Sigma^\dagger - i[v_\mu, \Sigma^\dagger], \tag{4}$$

with

$$\begin{aligned} v_\mu &= \delta_{\mu 0}\,\mathrm{diag}(\mu_u, \mu_d, \mu_s) \\ &= \delta_{\mu 0}\,\mathrm{diag}\left(\frac{1}{3}\mu_B + \frac{1}{2}\mu_I, \frac{1}{3}\mu_B - \frac{1}{2}\mu_I, \frac{1}{3}\mu_B - \mu_S\right), \end{aligned} \tag{5}$$

where $\mu_B = \frac{3}{2}(\mu_u + \mu_d)$, $\mu_I = \mu_u - \mu_d$, and $\mu_S = \frac{1}{2}(\mu_u + \mu_d - 2\mu_s)$. It turns out that the Lagrangian is independent of μ_B which reflects the fact that all degrees of freedom, namely the meson octet, have zero baryon number. Since we are focusing on pion condensation and want to compare with lattice data, we set $\mu_S = 0$ such that $v_0 = \frac{1}{2}\mu_I\lambda_3$. By expanding the Lagrangian (1) to second order in the fields, we obtain the terms needed for our NLO calculation.[1]

Based on the two-flavor case [23], the ground state in the pion-condensed phase is parametrized as [53]

$$\Sigma_\alpha = e^{i\alpha(\hat\phi_1\lambda_1 + \hat\phi_2\lambda_2)} = \cos\alpha + i(\hat\phi_1\lambda_1 + \hat\phi_2\lambda_2)\sin\alpha, \tag{6}$$

where α is a rotation angle and $\hat\phi_1^2 + \hat\phi_2^2 = 1$ to ensure that the ground state is normalized, $\Sigma_\alpha^\dagger\Sigma_\alpha = \mathbb{1}$. From Eq. (1), we find the static Hamiltonian

$$\begin{aligned} \mathcal{H}_2^{\mathrm{static}} = &\frac{f^2}{4}\mathrm{Tr}[v_0, \Sigma_\alpha][v_0, \Sigma_\alpha^\dagger] \\ &-\frac{f^2}{2}B_0\mathrm{Tr}[M\Sigma_\alpha + M\Sigma_\alpha^\dagger], \end{aligned} \tag{7}$$

where the first term can be written as $\frac{1}{4}f^2\mathrm{Tr}[v_0, \Sigma_\alpha][v_0, \Sigma_\alpha^\dagger] = \frac{1}{8}f^2\mu_I^2\mathrm{Tr}[\lambda_3\Sigma_\alpha\lambda_3\Sigma_\alpha^\dagger - \lambda_3^2]$. There is a competition between the two terms in Eq. (7): The first term favors Σ_α in the λ_1 and λ_2 directions, while Σ_α in the second terms prefers the normal vacuum, $\mathbb{1}$ [23]. It turns out the that the former only depends on $\hat\phi_1^2 + \hat\phi_2^2$ and so we choose $\hat\phi_2 = 1$ without loss of generality. The matrix λ_2 generates the rotations and the rotated vacuum is given by $\Sigma_\alpha = A_\alpha\Sigma_0 A_\alpha$ where $A_\alpha = e^{i\frac{\alpha}{2}\lambda_2}$, and $\Sigma_0 = \mathbb{1}$. The rotated vacuum can then be written in the form

$$\begin{aligned} \Sigma_\alpha &= \frac{1 + 2\cos\alpha}{3} + i\lambda_2\sin\alpha + \frac{\cos\alpha - 1}{\sqrt{3}}\lambda_8 \\ &= \begin{pmatrix} \cos\alpha & \sin\alpha & 0 \\ -\sin\alpha & \cos\alpha & 0 \\ 0 & 0 & 1 \end{pmatrix}. \end{aligned} \tag{8}$$

Here the rotation in the subspace of the u and the d-quark is evident and at tree level, we have $\langle\bar\psi\psi\rangle^2 + \langle\pi^+\rangle^2 = \langle\bar\psi\psi\rangle^2_{\mathrm{vac}}$, i.e. the quark condensate is rotated into a pion condensate.

The fluctuations around the condensed or rotated vacuum must also be parametrized and this requires some care [54]. Naively, one would write the field as $\Sigma = U\Sigma_\alpha U$, where $U = \exp\frac{i\lambda_i\phi_i}{2f}$. However, this parametrization is incorrect since it can be shown that one cannot renormalize the effective potential at next-to-leading order using the standard renormalization of the low-energy couplings appearing in the NLO Lagrangian. One way of understanding the failure of this parametrization is to realize that the generators of the fluctuations about the ground state must also be rotated since the vacuum itself has been rotated. The field must therefore be written as

[1] A covariant derivative and a mass term both count as order p in the low-energy expansion.

$$\Sigma = L_\alpha \Sigma_\alpha R_\alpha^\dagger \,, \tag{9}$$

where $L_\alpha = A_\alpha U A_\alpha^\dagger$ and $R_\alpha = A_\alpha^\dagger U^\dagger A_\alpha$. This parametrization reduces to the standard parametrization for $\alpha = 0$ and has none of the flaws of the naive parametrization.

The tree-level effective potential $V_0 = \mathcal{H}_2^{\rm static} = -\mathcal{L}^{\rm static}$ is now evaluated to be

$$V_0 = \quad -f^2 B_0(2m\cos\alpha + m_s) - \frac{1}{2} f^2 \mu_I^2 \sin^2\alpha \,. \tag{10}$$

At next-to-leading order in the low-energy expansion, there are twelve operators. Not all of them are relevant for the present calculations, in fact only eight contribute to the effective potential. They are

$$\begin{aligned}
\mathcal{L}_4 = {} & L_1 \left({\rm Tr}\left[\nabla_\mu \Sigma^\dagger \nabla^\mu \Sigma\right]\right)^2 \\
& + L_2 {\rm Tr}\left[\nabla_\mu \Sigma^\dagger \nabla_\nu \Sigma\right] {\rm Tr}\left[\nabla^\mu \Sigma^\dagger \nabla^\nu \Sigma\right] \\
& + L_3 {\rm Tr}\left[(\nabla_\mu \Sigma^\dagger \nabla^\mu \Sigma)(\nabla_\nu \Sigma^\dagger \nabla^\nu \Sigma)\right] \\
& + L_4 {\rm Tr}\left[\nabla_\mu \Sigma^\dagger \nabla^\mu \Sigma\right] {\rm Tr}\left[\chi^\dagger \Sigma + \chi \Sigma^\dagger\right] \\
& + L_5 {\rm Tr}\left[(\nabla_\mu \Sigma^\dagger \nabla^\mu \Sigma)\left(\chi^\dagger \Sigma + \Sigma^\dagger \chi\right)\right] \\
& + L_6 \left[{\rm Tr}\left(\chi^\dagger \Sigma + \chi \Sigma^\dagger\right)\right]^2 \\
& + L_8 {\rm Tr}\left[\chi^\dagger \Sigma \chi^\dagger \Sigma + \chi \Sigma^\dagger \chi \Sigma^\dagger\right] \\
& + H_2 {\rm Tr}[\chi^\dagger \chi] \,.
\end{aligned} \tag{11}$$

In writing the NLO Lagrangian above, we have ignored the Wess-Zumino-Witten terms since they do not contribute to the quantities in the present paper. The last term in Eq. (11) is a contact term, which is needed to renormalize the vacuum energy and to show the scale independence of the final result for the effective potential in each phase. The contribution from the terms in Eq. (11) to $\mathcal{H}_4^{\rm static} = -\mathcal{L}_4^{\rm static} = V_1^{\rm static}$ is

$$\begin{aligned}
V_1^{\rm static} = {} & -(4L_1 + 4L_2 + 2L_3)\mu_I^4 \sin^4\alpha \\
& - 8L_4 B_0(2m\cos\alpha + m_s)\mu_I^2 \sin^2\alpha \\
& - 8L_5 B_0 m \mu_I^2 \cos\alpha \sin^2\alpha \\
& - 16 L_6 B_0^2 (2m\cos\alpha + m_s)^2 \\
& - 8L_8 B_0^2 (2m^2\cos 2\alpha + m_s^2) \\
& - 4H_2 B_0^2 (2m^2 + m_s^2) \,.
\end{aligned} \tag{12}$$

In a next-to-leading order calculation, we need to renormalize the couplings L_i and H_i to eliminate the ultraviolet divergences that arise from the functional determinants. The relations between the bare and renormalized couplings are

$$L_i = L_i^r(\Lambda) - \Gamma_i \lambda \,, \tag{13}$$

$$H_i = H_i^r(\Lambda) - \Delta_i \lambda \,, \tag{14}$$

with $\lambda = \frac{\Lambda^{-2\epsilon}}{2(4\pi)^2}\left[\frac{1}{\epsilon} + 1\right]$. Here Γ_i and Δ_i are constants [21]

$$\Gamma_1 = \frac{3}{32} \,, \qquad \Gamma_2 = \frac{3}{16} \,, \qquad \Gamma_3 = 0 \,, \qquad \Gamma_4 = \frac{1}{8} \,, \tag{15}$$

$$\Gamma_5 = \frac{3}{8} \,, \qquad \Gamma_6 = \frac{11}{144} \,, \qquad \Gamma_8 = \frac{5}{48} \,, \qquad \Delta_2 = \frac{5}{24} \,, \tag{16}$$

and Λ is the renormalization scale associated with the modified minimal substraction scheme $\overline{\rm MS}$. Taking the derivative of Eqs. (13)–(14) and using the fact that the bare couplings are scale independent, one finds the renormalization group equations for the renormalized couplings,

$$\Lambda \frac{dL_i^r(\Lambda)}{d\Lambda} = -\frac{\Gamma_i}{(4\pi)^2} \,, \tag{17}$$

$$\Lambda \frac{dH_i^r(\Lambda)}{d\Lambda} = -\frac{\Delta_i}{(4\pi)^2} \,. \tag{18}$$

The contact term $H_2 {\rm Tr}[\chi^\dagger \chi]$ makes a constant contribution to the effective potential which is independent of the chemical potential and therefore the same in both phases. We keep it, however, in the final expression for the NLO effective potential since $H_2^r(\Lambda)$ is running. It is needed to show the scale independence of $V_{\rm eff}$. The renormalized NLO effective potential $V_{\rm eff} = V_0 + V_1 + V_1^{\rm static}$ is given by

$$\begin{aligned}
V_{\rm eff} = {} & -f^2 B_0(2m\cos\alpha + m_s) - \frac{1}{2} f^2 \mu_I^2 \sin^2\alpha \\
& - \Bigg[4L_1^r + 4L_2^r + 2L_3^r \\
& + \frac{1}{16(4\pi)^2}\left(\frac{9}{2} + 8\log\frac{\Lambda^2}{m_3^2} \right. \\
& \left. + \log\frac{\Lambda^2}{\tilde{m}_4^2}\right)\Bigg] \mu_I^4 \sin^4\alpha \\
& - \left[8L_4^r + \frac{1}{2(4\pi)^2}\left(\frac{1}{2} + \log\frac{\Lambda^2}{\tilde{m}_4^2}\right)\right] \\
& \times B_0(2m\cos\alpha + m_s)\mu_I^2 \sin^2\alpha \\
& - \left[8L_5^r + \frac{1}{2(4\pi)^2}\left(\frac{3}{2} + 4\log\frac{\Lambda^2}{m_3^2} - \log\frac{\Lambda^2}{\tilde{m}_4^2}\right)\right] \\
& \times B_0 m \mu_I^2 \cos\alpha \sin^2\alpha + B_0^2 m^2 \sin^2\alpha \left[16L_8^r - 8H_2^r\right] \\
& - \Bigg[16L_6^r + 8L_8^r + 4H_2^r + \frac{1}{(4\pi)^2}\left(\frac{13}{18} + \log\frac{\Lambda^2}{\tilde{m}_4^2} \right. \\
& \left. + \frac{4}{9}\log\frac{\Lambda^2}{m_8^2}\right)\Bigg] B_0^2 m_s^2 \\
& - \left[64L_6^r + \frac{1}{(4\pi)^2}\left(\frac{11}{9} + 2\log\frac{\Lambda^2}{\tilde{m}_4^2} + \frac{4}{9}\log\frac{\Lambda^2}{m_8^2}\right)\right] \\
& \times B_0^2 m m_s \cos\alpha \\
& - \Bigg[64L_6^r + 16L_8^r + 8H_2^r + \frac{1}{(4\pi)^2}\left(\frac{37}{18} + \log\frac{\Lambda^2}{\tilde{m}_1^2} + \right. \\
& \left. + 2\log\frac{\Lambda^2}{m_3^2} + \log\frac{\Lambda^2}{\tilde{m}_4^2} + \frac{1}{9}\log\frac{\Lambda^2}{m_8^2}\right)\Bigg] B_0^2 m^2 \cos^2\alpha \\
& + V_{1,\pi^+}^{\rm fin} + V_{1,\pi^-}^{\rm fin} \,,
\end{aligned} \tag{19}$$

where $L_i^r(\Lambda)$ are the renormalized coupling constants and the masses are

$$\tilde{m}_1^2 = 2B_0 m\cos\alpha \,, \tag{20}$$

$$m_3^2 = 2B_0 m\cos\alpha + \mu_I^2 \sin^2\alpha \,, \tag{21}$$

$$\tilde{m}_4^2 = B_0(m\cos\alpha + m_s) + \frac{1}{4}\mu_I^2 \sin^2\alpha \,, \tag{22}$$

$$m_8^2 = \frac{2B_0(m\cos\alpha + 2m_s)}{3} \,. \tag{23}$$

Finally, $V^{\rm fin}_{1,\pi^\pm}$ are finite subtraction terms which depend on B_0 and m but are independent of m_s. For details, see Ref. [53]. The couplings are running in such a way that their Λ-dependence cancel against the explicit Λ-dependence of the chiral logarithms in Eq. (19), implying that $\Lambda\frac{dV_{\rm eff}}{d\Lambda}=0$, cf. Eqs. (17)–(18). In order to obtain Eq. (19), we must isolate the ultraviolet divergences from the functional determinants. This is done by adding and subtracting a divergent term that we calculate analytically in dimensional regularization. The subtracted term is then combined with the original one-loop expression for the effective potential giving finite terms $V^{\rm fin}_{1,\pi^\pm}$ that can be easily computed numerically. The divergences are finally removed by renormalization of the L_is according to Eqs. (13)–(14). The details of the subtraction and renormalization procedure can be found in Ref. [53] and the NLO effective potential in the two-flavor case can be found in Ref. [52].

Thermodynamic quantities can be calculated from the effective potential Eq. (19), for example the pressure $P=-V_{\rm eff}$, the isospin density $n_I=-\frac{\partial V_{\rm eff}}{\partial\mu_I}$, and the energy density $\epsilon=-P+n_I\mu_I$. All these quantities are evaluated at the value of α that minimizes the effective potential, i.e. satisfies $\frac{\partial V_{\rm eff}}{\partial\alpha}=0$.

For sufficiently large values of m_s, we expect using effective-field theory arguments, that all degrees of freedom that contain an s-quark freeze and decouple. Thus we expect that the kaons and eta decouple from the low-energy dynamics involving the pions. Formally, this is the limit $B_0m\ll B_0m_s\ll(4\pi f_\pi)^2$. The system is then described in terms of two-flavor chiral perturbation theory where the effects of the s-quark shows up in the renormalization of the coupling constants l_i of the form $\log\frac{\Lambda^2}{\tilde m^2_{K,0}}$ and $\log\frac{\Lambda^2}{\tilde m^2_{\eta,0}}$, where the masses are $\tilde m^2_{K,0,}=B_0m_s$ and $\tilde m^2_{\eta,0}=\frac{4B_0m_s}{3}$. Expanding the effective potential Eq. (19) in inverse powers of m_s, we obtain

$$
\begin{aligned}
V_{\rm eff}=&-2\tilde f^2\tilde B_0m\cos\alpha-f^2B_0m_s-\frac{1}{2}\tilde f^2\mu_I^2\sin^2\alpha\\
&-\left[4l_3^r+4l_4^r+\frac{1}{(4\pi)^2}\left(\frac{3}{2}+\log\frac{\Lambda^2}{\tilde m_1^2}\right.\right.\\
&\left.\left.+2\log\frac{\Lambda^2}{m_3^2}\right)\right]B_0^2m^2\cos^2\alpha\\
&-\left[l_4^r+\frac{1}{(4\pi)^2}\left(\frac{1}{2}+\log\frac{\Lambda^2}{m_3^2}\right)\right]\\
&\times2B_0m\mu_I^2\cos\alpha\sin^2\alpha\\
&-\left[l_1^r+l_2^r+\frac{1}{2(4\pi)^2}\left(\frac{1}{2}+\log\frac{\Lambda^2}{m_3^2}\right)\right]\mu_I^4\sin^4\alpha\\
&+4(-h_1^r+l_4^r)B_0^2m^2-\big[16L_6^r+8L_8^r+4H_2^r\\
&+\frac{1}{(4\pi)^2}\left(\frac{13}{18}+\log\frac{\Lambda^2}{\tilde m^2_{K,0}}\right.\\
&\left.+\frac{4}{9}\log\frac{\Lambda^2}{\tilde m^2_{\eta,0}}\right)\Big]B_0^2m_s^2+V^{\rm fin}_{1,\pi^+}+V^{\rm fin}_{1,\pi^-}\,,
\end{aligned}
\tag{24}
$$

where we have defined the combinations of the renormalized couplings l_i^r and h_1^r as well as renormalized $\tilde f$ and $\tilde B_0$ as

$$
\begin{aligned}
l_1^r+l_2^r=&\,4L_1^r+4L_2^r+2L_3^r\\
&+\frac{1}{16(4\pi)^2}\left[\log\frac{\Lambda^2}{\tilde m^2_{K,0}}-1\right],
\end{aligned}
\tag{25}
$$

$$
\begin{aligned}
l_3^r+l_4^r=&\,16L_6^r+8L_8^r+\frac{1}{4(4\pi)^2}\left[\log\frac{\Lambda^2}{\tilde m^2_{K,0}}-1\right]\\
&+\frac{1}{36(4\pi)^2}\left[\log\frac{\Lambda^2}{\tilde m^2_{\eta,0}}-1\right],
\end{aligned}
\tag{26}
$$

$$
l_4^r=8L_4^r+4L_5^r+\frac{1}{4(4\pi)^2}\left[\log\frac{\Lambda^2}{\tilde m^2_{K,0}}-1\right],
$$

$$
-h_1^r+l_4^r=4L_8^r-2H_2^r\,,
\tag{27}
$$

$$
\begin{aligned}
\tilde f^2=&\,f^2\left[1+\frac{B_0m_s}{f^2}\left(16L_4^r\right.\right.\\
&\left.\left.+\frac{1}{(4\pi)^2}\log\frac{\Lambda^2}{\tilde m^2_{K,0}}\right)\right],
\end{aligned}
\tag{28}
$$

$$
\begin{aligned}
\tilde B_0=&\,B_0\left[1-\frac{B_0m_s}{f^2}\left(16L_4^r-32L_6^r-\right.\right.\\
&\left.\left.\frac{2}{9(4\pi)^2}\log\frac{\Lambda^2}{\tilde m^2_{\eta,0}}\right)\right].
\end{aligned}
\tag{29}
$$

Several comments are in order: The terms in Eq. (24) that are proportional to powers of m_s are independent of α and μ_I. They can be interpreted as a constant renormalized contribution to the vacuum energy from the s-quark and can be omitted. The constant term proportional to $B_0^2m^2$ can be omitted for similar reasons. The relations between the renormalized couplings l_i^r, h_i^r and the low-energy constants $\bar l_i, \bar h_i$ in two-flavor χPT are

$$
l_i^r(\Lambda)=\frac{\gamma_i}{2(4\pi)^2}\left[\bar l_i+\log\frac{2B_0m}{\Lambda^2}\right],
\tag{30}
$$

$$
h_i^r(\Lambda)=\frac{\delta_i}{2(4\pi)^2}\left[\bar h_i+\log\frac{2B_0m}{\Lambda^2}\right],
\tag{31}
$$

where $\gamma_1=\frac{1}{3}$, $\gamma_2=\frac{2}{3}$, $\gamma_3=-\frac{1}{2}$, $\gamma_4=2$, and $\delta_1=2$ [20]. The renormalization group equations are then $\Lambda\frac{dl_i^r(\Lambda)}{d\Lambda}=-\frac{\gamma_i}{(4\pi)^2}$. Given the renormalization group equations for l_i^r, h_i^r, L_i^r, H_i^r, one verifies that the Λ-dependence of the left - and right-hand side in Eqs. (25)–(27) is identical. Moreover, the parameters $\tilde f$ and $\tilde B_0$ are independent of the scale. Eqs. (25)–(29) are in agreement with the original calculations of Ref. [21], where relations among the renormalized couplings in two - and three-flavor χPT were derived. This agreement is a nontrivial check of our calculations. Inserting these relations using (31) into Eq. (24), we finally obtain

$$
\begin{aligned}
V_{\rm eff}=&-2\tilde f^2\tilde B_0m\cos\alpha-\frac{1}{2}\tilde f^2\mu_I^2\sin^2\alpha\\
&-\frac{1}{(4\pi)^2}\left[\frac{3}{2}-\bar l_3+4\bar l_4+\log\left(\frac{2B_0m}{\tilde m_1^2}\right)\right.\\
&\left.+2\log\left(\frac{2B_0m}{m_3^2}\right)\right]B_0^2m^2\cos^2\alpha\\
&-\frac{1}{(4\pi)^2}\left[\frac{1}{2}+\bar l_4+\log\left(\frac{2B_0m}{m_3^2}\right)\right]\\
&\times2B_0m\mu_I^2\cos\alpha\sin^2\alpha\\
&-\frac{1}{2(4\pi)^2}\left[\frac{1}{2}+\frac{1}{3}\bar l_1+\frac{2}{3}\bar l_2+\log\left(\frac{2B_0m}{m_3^2}\right)\right]\\
&\times\mu_I^4\sin^4\alpha+V^{\rm fin}_{1,\pi^+}+V^{\rm fin}_{1,\pi^-}\,.
\end{aligned}
\tag{32}
$$

In the limit $B_0 m_s \ll (4\pi f_\pi)^2$, B_0 in the NLO terms can be identified with $\tilde{B}_0$ using Eq. (29) and the result reduces to that of two-flavor χPT in Ref. [52].

3. Results and discussion

The expressions for the effective potential, isospin density, pressure, and energy density are all expressed in terms of the isospin chemical potential, the parameters $B_0 m$, $B_0 m_s$, and f of the chiral Lagrangian as well as the renormalized couplings L_i^r. In order to make predictions, we need to determine the parameters of the chiral Lagrangian using the physical meson masses and the decay constants. In χPT, one can calculate the pole masses of the mesons and the decay constants (f_π, f_K) systematically in the low-energy expansion. At one loop, the results are expressed in terms of $B_0 m$, $B_0 m_s$, f, and L_i^r.[2] These equations can be solved to find the parameters of the chiral Lagrangian and thereby numerically evaluate the effective potential. The tree-level values of $m_{\pi,0}$ and $m_{K,0}$ can be expressed in terms of $B_0 m$ and $B_0 m_s$ as $m_{\pi,0}^2 = 2B_0 m$ and $m_{K,0}^2 = B_0(m + m_s)$. Since we want to compare our predictions with the results of the lattice simulations, we use their values for the meson masses and decay constants [55],

$$m_\pi = 131 \pm 3\ \text{MeV}\,, \qquad m_K = 481 \pm 10\ \text{MeV}\,, \tag{33}$$

$$f_\pi = \frac{128 \pm 3}{\sqrt{2}}\text{MeV}\,, \qquad f_K = \frac{150 \pm 3}{\sqrt{2}}\text{MeV}. \tag{34}$$

The low-energy constants have been determined experimentally, with the following values and uncertainties at the scale $\mu = m_\rho$, where m_ρ is the mass of the ρ meson and $\Lambda^2 = 4\pi e^{-\gamma_E}\mu^2$ [56]

$$L_1^r = (1.0 \pm 0.1) \times 10^{-3} \qquad L_2^r = (1.6 \pm 0.2) \times 10^{-3} \tag{35}$$

$$L_3^r = (-3.8 \pm 0.3) \times 10^{-3} \qquad L_4^r = (0.0 \pm 0.3) \times 10^{-3} \tag{36}$$

$$L_5^r = (1.2 \pm 0.1) \times 10^{-3} \qquad L_6^r = (0.0 \pm 0.4) \times 10^{-3} \tag{37}$$

$$L_8^r = (0.5 \pm 0.2) \times 10^{-3}\,. \tag{38}$$

Since we need to determine three parameters in the effective potential, we must choose three of the four physical quantities from Eqs. (33)–(34). For the results that we present below, we use m_π, m_K, and f_π. Using the one-loop χPT expression for f_K, we obtain $f_K = 113.9$ MeV for the central value, which is off by approximately 7% compared to the lattice value of $f_K = \frac{150}{\sqrt{2}} = 106.1$ MeV. The uncertainties in L_i^r, m_π, m_K, and f_π translate into uncertainties in the parameters $B_0 m$, $B_0 m_s$, and f. It turns out that the uncertainties in these parameters in the three-flavor case are completely dominated by the uncertainties in the LECs. In the two-flavor case, they are dominated by the uncertainties in the pion mass and the pion decay constant. Furthermore, for the lowest values of LECs obtained using the largest uncertainties in Eq. (38), the η mass becomes imaginary and therefore unphysical. Consequently, we are forced to restrict the smallest value of the LECs used to ones obtained using 46% of the total uncertainty. We therefore simplify the analysis and add the uncertainties. This yields

$$m_{\pi,0}^{\text{cen}} = 131.28\ \text{MeV} \qquad m_{K,0}^{\text{cen}} = 520.65\ \text{MeV} \tag{39}$$

$$m_{\pi,0}^{\text{low}} = 148.45\ \text{MeV} \qquad m_{K,0}^{\text{low}} = 617.35\ \text{MeV} \tag{40}$$

$$m_{\pi,0}^{\text{high}} = 115.93\ \text{MeV} \qquad m_{K,0}^{\text{high}} = 437.84\ \text{MeV} \tag{41}$$

$$f^{\text{cen}} = 75.16\ \text{MeV} \tag{42}$$

[2] All the relevant relationships between bare and physical quantities (masses and decay constants) are stated in Ref. [21].

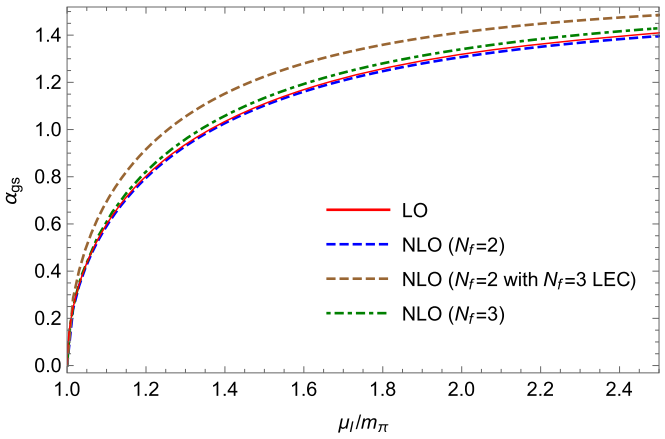

Fig. 1. α_{gs} as a function of μ_I/m_π at LO (red), at NLO with two flavors (blue), NLO with three flavors (green), and NLO with two flavors and three-flavor LECs (brown). See main text for details.

$$f^{\text{low}} = 79.88\ \text{MeV} \tag{43}$$

$$f^{\text{high}} = 70.44\ \text{MeV}\,. \tag{44}$$

Given that the effective potential derived in three-flavor χPT of Eq. (19) reduces to the result in two-flavor χPT, in the limit of light up and down quarks, it is worthwhile comparing the predictions from two-flavor χPT from Ref. [52] using the $N_f = 2$ LECs from the literature and those obtained by using Eqs. (25)–(27). The $N_f = 2$ LECs have the following values[3] [56]

$$\bar{l}_1(N_f = 2) = -0.4 \qquad \bar{l}_2(N_f = 2) = 4.3 \tag{45}$$

$$\bar{l}_3(N_f = 2) = 2.9 \qquad \bar{l}_4(N_f = 2) = 4.4\,. \tag{46}$$

The three-flavor LECs L_i^r are the running couplings evaluated at the scale m_ρ and we use their renormalization group equations to run them to the scale $m_{\pi,0}$, where the two-flavor LECs ($\bar{l}_i$), defined in Eq. (31), are evaluated according to Eqs. (25)–(27). We then get the following central values

$$\bar{l}_1(N_f = 3) = 14.5 \qquad \bar{l}_2(N_f = 3) = 6.5 \tag{47}$$

$$\bar{l}_3(N_f = 3) = 4.1 \qquad \bar{l}_4(N_f = 3) = 4.2\,. \tag{48}$$

The disagreement is most significant in $\bar{l}_1$, which in the two-flavor versus the three-flavor case, have signs that are opposite. The differences in the other LECs are less significant but still non-trivial except for $\bar{l}_4$. In order to evaluate the effect of these discrepancies on physical observables in the pion-condensed phase, we have generated the isospin density, pressure, and the equation of state using the two-flavor LEC values generated using three-flavor LECs, which we discuss at the end of this section.

The equation $\frac{\partial V_{\text{eff}}}{\partial \alpha} = 0$ has two types of solutions. For $\mu_I < m_\pi$, the solution is $\alpha = 0$, where it is straightforward to show that the effective potential and therefore the thermodynamic functions are independent of μ_I. We refer to this phase as the vacuum phase, which exhibits the Silver Blaze property [57], namely that the thermodynamic functions are independent of μ_I up to a critical value $\mu_I^c = m_\pi$. For $\mu_I > m_\pi$, we have a nonzero condensate of π^+, which breaks the $U(1)_{I_3}$ symmetry of the chiral Lagrangian, and a nonzero value for α. In Fig. 1, we show the solution α_{gs} to the

[3] We note that it is standard practice to quote the LECs in two-flavor χPT using $\bar{l}_i$ defined through Eq. (31). On the other hand, for three-flavor χPT, quoting L_i^r at the scale μ equal to the ρ mass (m_ρ) is standard.

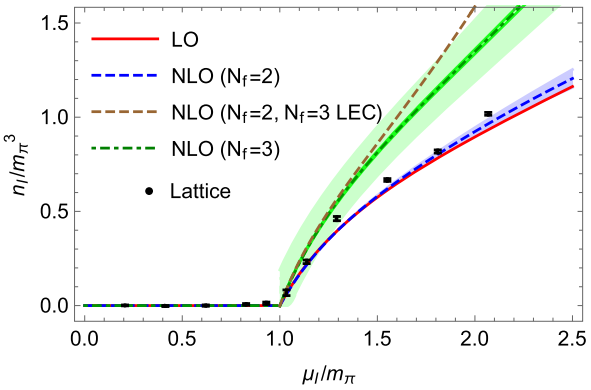

Fig. 2. Normalized isospin density as a function of μ_I/m_π at LO (red), at NLO with two flavors (blue), NLO with three flavors (green), and NLO with two flavors and three-flavor LECs (brown). See main text for details.

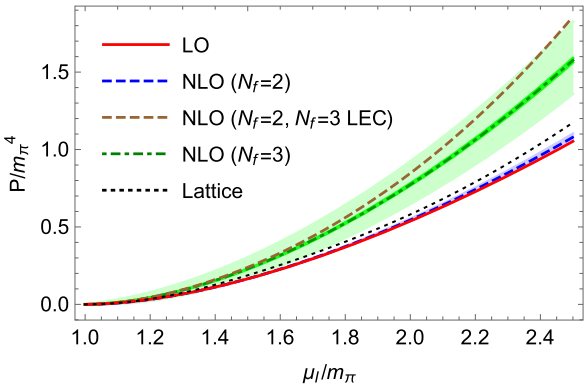

Fig. 3. Pressure normalized by m_π^4 as a function of μ_I/m_π at LO (red), at NLO with two flavors (blue), NLO with three flavors (green), and NLO with two flavors and three-flavor LECs (brown). See main text for details.

equation $\frac{\partial V_{\rm eff}}{\partial \alpha} = 0$ as a function of $\frac{\mu_I}{m_\pi}$ at LO.[4] For asymptotically large values of the isospin chemical, $\alpha_{\rm gs}$ approaches $\frac{\pi}{2}$.

We next expand the effective potential around $\alpha = 0$ to obtain a Ginzburg-Landau energy functional that can be used to determine the order of the phase transition. This expansion is valid close to the phase transition where $\alpha \ll 1$. To fourth-order, we obtain [53]

$$V_{\rm eff}^{\rm LG} = a_0(\mu_I) + a_2(\mu_I)\alpha^2 + a_4(\mu_I)\alpha^4 \,. \tag{49}$$

The vanishing of a_2 defines the critical chemical potential μ_I^c. Since $a_2 = f_\pi^2(\mu_I^2 - m_\pi^2)$, we have $\mu_I^c = m_\pi$. The onset of Bose condensation at $\mu_I^c = m_\pi$ is an exact result. Moreover, since the coefficient $a_4(\mu_I^c) > 0$, the transition to a pion-condensed phase is of second order, with mean field critical exponents. These results are in agreement with lattice simulations [15–17] as well as model calculations [51].

In Fig. 2, we show the isospin n_I divided by m_π^3 as a function of μ_I/m_π. The red solid line is the LO result. Note that the LO result is the same in the two and three-flavor cases for all thermodynamic quantities. We have used the central values for the low-energy constants $\bar{l}_i$ in the two-flavor case to obtain the blue dashed line as explained in Ref. [52]. The blue band is obtained by including their uncertainties. The light green band is the result of the three-flavor calculation with the minimum, central, and maximum values of the parameters discussed above, while the dark green band is from using the central values of L_i^r with uncertainties coming from the lattice parameters only.

The data points shown in Fig. 2 are from the lattice calculations of Refs. [15–17]. The two-flavor band is very small compared to the three-flavor band reflecting the large uncertainty in the three-flavor L_i^rs. The central line in the three-flavor case is in very good agreement with lattice data up to approximately $\mu_I \sim 200$ MeV. After this, the curve overshoots and for larger values the two-flavor central curve is in much better agreement with lattice data.

In Fig. 3, we show the pressure P divided by m_π^4 as a function of μ_I/m_π. Note that we have subtracted the pressure in the vacuum phase which is given by evaluating the negative of Eq. (19) for $\alpha = 0$. The red line is the LO result. The blue dashed line is again the result from two-flavor χPT using the central values of $\bar{l}_i$, while the band is obtained by including their uncertainties. Similarly, the dashed-dotted line corresponds to the central values of the L_i^rs in the three-flavor case, while the light green band is obtained by including their uncertainties. Finally, by including only the uncertainties from the lattice parameters we obtain the much narrower dark green band. Here, the LO and the two-flavor results

[4] At LO, the two and three-flavor results for α coincide.

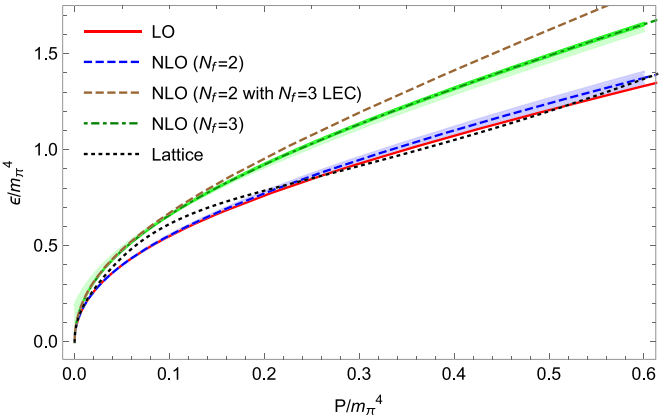

Fig. 4. Energy density as a function of pressure, both normalized by m_π^4, at LO (red), at NLO with two flavors (blue), NLO with three flavors (green), and NLO with two flavors and three-flavor LECs (brown). See main text for details.

very close in the entire range and systematically slightly below the lattice data. The three-flavor curve is in very good agreement with the results of the Monte Carlo simulations up to $\mu_I = 200$ MeV, after which it overestimates the pressure.

In Fig. 4, we show the energy density ϵ divided by m_π^4 as a function of pressure P divided by m_π^4. For all values of $\frac{P}{m_\pi^4}$ three-flavor χPT overestimates the energy density compared to lattice data though for values of $\frac{P}{m_\pi^4}$ up to approximately 0.10, the discrepancy is quite small. On the other hand, two-flavor χPT underestimates the energy density as a function of pressure for values of $\frac{P}{m_\pi^4}$ up to 0.20. For values larger than approximately 0.20, two-flavor χPT agrees very well with lattice results.

Given the results shown in Figs. 2, 3 and 4 above, in particular the large differences between the results in two-flavor and three-flavor χPT and the results in lattice QCD compared to three-flavor χPT, it is important to explain this significant discrepancy. The naive expectation is that the loop effects from the strange quarks in three-flavor χPT are small since the effect is sub-leading in the chiral expansion. Furthermore, their effects should be suppressed since the strange quark mass is considerably larger than the masses of the up and down quarks. While this picture is correct, it ignores the significant differences between the low energy constants of two-flavor χPT and the ones that are extracted from three-flavor χPT after integrating out the effect of the strange quarks. We list the values in Eqs. (45) and (47) noting significant discrepancies between the two sets. In each of the figures (2, 3 and 4), we incorporate an additional result in two-flavor χPT using

three-flavor LECs shown using brown and dashed lines. We note that even two-flavor χPT using three-flavor LECs overestimates the isospin density, pressure and the energy density compared to lattice QCD results. For isospin chemical potential near the second order phase transition up to approximately $\frac{\mu_I}{m_\pi} \sim 1.3$, the differences in the LECs fully explains the discrepancy. For larger values of isospin chemical potential, the role of strange quark loops becomes more significant – our results suggests that they have a negative effect on the pressure and isospin density compared to the effects of the up and down quarks.

Declaration of competing interest

There is no conflict of interest.

Acknowledgements

The authors would like to thank B. Brandt, G. Endrődi, and S. Schmalzbauer for useful discussions as well as for providing the data points of Ref. [17].

References

[1] K. Rajagopal, F. Wilczek, At the Frontier of Particle Physics, vol. 3, World Scientific, Singapore, 2001, p. 2061.
[2] M.G. Alford, A. Schmitt, K. Rajagopal, T. Schäfer, Rev. Mod. Phys. 80 (2008) 1455.
[3] K. Fukushima, T. Hatsuda, Rep. Prog. Phys. 74 (2011) 014001.
[4] S. Borsanyi, G. Endrődi, Z. Fodor, S.D. Katz, S. Krieg, C. Ratti, K.K. Szabo, J. High Energy Phys. 1208 (2012) 053.
[5] B.A. Freedman, L.D. McLerran, Phys. Rev. D 16 (1977) 1147.
[6] B.A. Freedman, L.D. McLerran, Phys. Rev. D 16 (1977) 1169.
[7] A. Kurkela, P. Romatscke, A. Vuorinen, Phys. Rev. D 81 (2010) 105021.
[8] T. Gorda, A. Kurkela, P. Romatschke, M. Säppi, A. Vuorinen, Phys. Rev. Lett. 121 (2018) 202701.
[9] G. Baym, T. Hatsuda, T. Kojo, P.D. Powell, Y. Song, T. Takatsuka, Rep. Prog. Phys. 81 (2018) 056902.
[10] S. Cotter, P. Giudice, S. Hands, J.-I. Skullerud, Phys. Rev. D 87 (2013) 034507.
[11] S. Hands, I. Montvay, S. Morrison, M. Oevers, L. Scorzato, J.-I. Skullerud, Eur. Phys. J. C 17 (2000).
[12] G.S. Bali, F. Bruckmann, G. Endrodi, Z. Fodor, S.D. Katz, S. Krieg, A. Schafer, K.K. Szabo, J. High Energy Phys. 1202 (2012) 044.
[13] J.B. Kogut, D.K. Sinclair, Phys. Rev. D 66 (2002) 014508.
[14] J.B. Kogut, D.K. Sinclair, Phys. Rev. D 66 (2002) 034505.
[15] B.B. Brandt, G. Endrődi, PoS LATTICE 2016 (2016) 039.
[16] B.B. Brandt, G. Endrődi, S. Schmalzbauer, EPJ Web Conf. 175 (2018) 07020.
[17] B.B. Brandt, G. Endrődi, S. Schmalzbauer, Phys. Rev. D 97 (2018) 054514.
[18] M. Mannarelli, Particles 2 (2019) 411.
[19] S. Weinberg, Physica A 96 (1979) 327.
[20] J. Gasser, H. Leutwyler, Ann. Phys. 158 (1984) 142.
[21] J. Gasser, H. Leutwyler, Nucl. Phys. B 250 (1985) 465.
[22] J. Bijnens, G. Colangelo, G. Ecker, Ann. Phys. 280 (2000) 100.
[23] D.T. Son, M.A. Stephanov, Phys. Rev. Lett. 86 (2001) 592.
[24] J.B. Kogut, D. Toublan, Phys. Rev. D 64 (2001) 034007.
[25] K. Splittorff, D. Toublan, J.J.M. Verbaarschot, Nucl. Phys. B 620 (2002) 290.
[26] M. Loewe, C. Villavicencio, Phys. Rev. D 67 (2003) 074034.
[27] E.S. Fraga, L.F. Palhares, C. Villavicencio, Phys. Rev. D 79 (2009) 014021.
[28] T.D. Cohen, S. Sen, Nucl. Phys. A 942 (2015) 39.
[29] O. Janssen, M. Kieburg, K. Splittorff, J.J.M. Verbaarschot, S. Zafeiropoulos, Phys. Rev. D 93 (2016) 094502.
[30] S. Carignano, A. Mammarella, M. Mannarelli, Phys. Rev. D 93 (2016) 051503.
[31] S. Carignano, L. Lepori, A. Mammarella, M. Mannarelli, G. Pagliaroli, Eur. Phys. J. A 53 (2017) 35.
[32] L. Lepori, M. Mannarelli, Phys. Rev. D 99 (2019) 096011.
[33] M. Frank, M. Buballa, M. Oertel, Phys. Lett. B 562 (2003) 221.
[34] D. Toublan, J.B. Kogut, Phys. Lett. B 564 (2003) 212.
[35] A. Barducci, R. Casalbuoni, G. Pettini, L. Ravagli, Phys. Rev. D 69 (2004) 096004.
[36] L. He, P.-F. Zhuang, Phys. Lett. B 615 (2005) 93.
[37] L. He, M. Jin, P.-F. Zhuang, Phys. Rev. D 71 (2005) 116001.
[38] L. He, M. Jin, P.-F. Zhuang, Phys. Rev. D 74 (2006) 036005.
[39] D. Ebert, K.G. Klimenko, J. Phys. G 32 (2006) 599.
[40] D. Ebert, K.G. Klimenko, Eur. Phys. J. C 46 (2006) 771.
[41] G.-F. Sun, L. He, P.-F. Zhuang, Phys. Rev. D 75 (2007) 096004.
[42] J.O. Andersen, L. Kyllingstad, J. Phys. G 37 (2009) 015003.
[43] H. Abuki, R. Anglani, R. Gatto, M. Pellicoro, M. Ruggieri, Phys. Rev. D 79 (2009) 034032.
[44] C.-F. Mu, L. He, Y. Liu, Phys. Rev. D 82 (2010) 056006.
[45] T. Xia, L. He, P. Zhuang, Phys. Rev. D 88 (2013) 056013.
[46] S.S. Avancini, A. Bandyopadhyay, D.C. Duarte, R.L.S. Farias, Phys. Rev. D 100 (2019) 116002.
[47] Z.-Y. Lu, C.-J. Xia, M. Ruggieri, Eur. Phys. J. C 80 (2020) 46.
[48] K. Kamikado, N. Strodthoff, L. von Smekal, J. Wambach, Phys. Lett. B 718 (2013) 1044.
[49] H. Ueda, T.Z. Nakano, A. Ohnishi, M. Ruggieri, K. Sumiyoshi, Phys. Rev. D 88 (2013) 074006.
[50] R. Stiele, E.S. Fraga, J. Schaffner-Bielich, Phys. Lett. B 729 (2014) 72.
[51] P. Adhikari, J.O. Andersen, P. Kneschke, Phys. Rev. D 98 (2018) 074016.
[52] P. Adhikari, J.O. Andersen, P. Kneshcke, Eur. Phys. J. C 79 (2019) 874.
[53] P. Adhikari, J.O. Andersen, arXiv:1909.10575.
[54] K. Splittorff, D.T. Son, M.A. Stephanov, Phys. Rev. D 64 (2001) 016003.
[55] G. Endrődi, private communication.
[56] J. Bijnens, G. Ecker, Annu. Rev. Nucl. Part. Sci. 64 (2014) 149.
[57] T.D. Cohen, Phys. Rev. Lett. 91 (2003) 222001.